Simulation of vegetation feedbacks on local and regional scale precipitation in West Africa

Authors: Andrew J. Hartley[12*], Douglas J. Parker[3], Luis Garcia-Carreras[3], and Stuart Webster[1]

For submission to: Agricultural and Forest Meteorology

Acknowledgements: The work was funded via the academic partnership between the Met Office and Leeds University. We also acknowledge Debbie Hemming[1] and Stephen Sitch[3] for help and support in the preparation of this work. This research was also funded by NERC and DfID under the AMMA-2050 project; grant reference number NE/M020428/1

* **Corresponding author:** Andrew J. Hartley; telephone: +44 (0) 1392 885720 ; email: andrew.hartley@metoffice.gov.uk and ajh235@exeter.ac.uk

Keywords

West Africa; Mesoscale Convective Systems; Vegetation feedbacks; Land use change

Abstract

Planned changes to land use in West Africa have been proposed to both combat desertification and to preserve biodiversity in the region, however, there is an urgent need for tools to assess the effects of these proposed changes on local and

[1] Met Office Hadley Centre, FitzRoy Road, Exeter, UK
[2] Department of Geography, University of Exeter, Exeter, UK
[3] Institute for Climate and Atmospheric Science, University of Leeds, Leeds, UK

regional scale precipitation. We use a high-resolution, convection-permitting numerical weather prediction (NWP) model to study how the initiation and propagation of mesoscale convective systems (MCS) depends on the surface vegetation cover. The simulations covered a 4-day period during the West African monsoon in August 2006. In many aspects of the simulations, there was evidence of vegetation type exerting a significant influence on the location of precipitation where the influence of orography and coastal water was minimal. In this study, vegetation was classified according to the fractional coverage of tree (>30%) and grass (>30%) plant functional types. Tree-grass boundary cover was defined where more than 3 grid cells of both tree and grass occurred in a moving 3x3 window, which was further enlarged using a 3 grid cell (~12km) buffer. We found that over the whole study region (5N to 17N and 11W to 9E) 33.8% of convective initiations occur over tree-grass boundaries that cover only 28.4% of the land surface. This is significantly more than would be expected by chance ($p = 0.0483$), providing support to the hypothesis that vegetation gradients provide heat and moisture gradients, of a similar magnitude to that of soil moisture. Additionally, we found that on average, more time under an MCS occurred over boundary cover and orography, followed by tree cover, during the afternoon and evening period, thus supporting the hypothesis that land cover type influences the location of larger propagating systems. Contrasting patterns were found in the quantity of precipitation between small-scale convective cells and larger scale MCS. More small-scale precipitation accumulated, on average, over grass cover during the afternoon period, indicating a tendency for small-scale convection, initiated over boundaries, to prefer the drier and warmer grass side of vegetation boundaries in the afternoon period. However, once these

smaller scale convective cells merge together to form larger MCS, a tendency for the most intense precipitation to fall over tree cover was observed. When intense precipitation (>10mm per hour) occurred simultaneously over tree, boundary and grass cover, we found the highest precipitation rate to be most frequently over tree cover (48.4%), and least frequently over boundary cover (19.9%), indicating a preference of MCS for cooler, more moist forest cover. These results show for the first time that convection-permitting NWP models do exhibit responses to vegetation similar to those observed in the real world, and therefore are useful tools to assess the impacts of proposed future land use changes.

Introduction

Human induced land use change has been well documented to have feedbacks to the climate system in simulations of global and continental scale climate change [*Mahmood et al.*, 2014]. Increasing observational evidence points towards vegetation in the tropics having an influence over the atmospheric boundary layer at length scales of up to 10km [*Garcia-Carreras et al.*, 2010; *Knox et al.*, 2011]. Such spatial scales are beyond the scope of most climate models, but the potential for vegetation to exert further influence on local and regional precipitation patterns via high-resolution feedback processes has yet to be fully explored.

Land use change is occurring rapidly in many parts of West Africa, including deforestation, as well as planned and unplanned afforestation [*Hansen et al.*, 2013] with little understanding as to the effects that changes in forest cover may have on monsoon rainfall. For example, plans to construct a Great Green Wall across the Sahel to combat desertification may have unintended consequences for local precipitation patterns. If we are to offer advice to land use planners in the region on the consequences of large-scale changes to the vegetation, we need models that are capable of capturing the observed interactions between the land surface and the boundary layer. There are large uncertainties in the effects of land use change on tropical precipitation, possibly related to issues of the scale of processes involved, but also very strongly related to the representation of convection. [*Taylor et al.*, 2013] show that convective representation is a much stronger control on the statistical relationship of rainfall with the land surface, than model resolution. Indeed, the response of rainfall to the land-surface state seems to have the wrong sign in GCMs [*Taylor et al.*, 2012], and this incorrect response has been shown to be due to the failure of parameterised convection schemes to faithfully locate convection according to surface and low-level conditions [*Taylor et al.*, 2013].

Observational studies have shown that strong gradients of heat and moisture can occur on vegetation boundaries such as those between cropland and forest [*Shaw and Doran*, 2001; *Garcia-Carreras et al.*, 2010]. Low-level horizontal pressure gradients are created by generally greater transpiration and soil evaporation associated with forest cover compared to cropland, and higher albedo and land surface temperatures associated with croplands compared to forest cover. These low-level thermal gradients can induce 'vegetation breezes' as simulated by [*Letzel and Raasch*, 2003; *Kang and Bryan*, 2011] which in turn can control the occurrence of convection in two ways [*Garcia-Carreras et al.*, 2011]. Firstly, the convergence provided by the vegetation breeze leads to upward motion that, through nonlinear dynamics of the flow, is strong enough to overcome convective inhibition (CIN) and initiate convection [*Segal and Arritt*, 1992]. Secondly, the convergence also concentrates low level humidity, reducing dry entrainment from above, and therefore maximises the equivalent potential temperature (θe) in the convergence zone close to the vegetation boundary [*Garcia-Carreras et al.*, 2011]. This θe maximum provides high convective available potential energy (CAPE) and low CIN, for the initiation of local scale convection. In idealised modelling studies, it was also found that the breeze circulations lead to subsidence on the cool side of the vegetation boundary, causing a significant (half) reduction in the rainfall over the remaining forest [*Garcia-Carreras and Parker,* 2011].

If convective storms achieve significant size and longevity, they are termed meso-scale convective systems (MCS). MCS can contribute between 80-90% of annual precipitation to parts of the Sahel [*Mathon and Laurent,* 2001]. However, in more southerly parts of West Africa, MCS may deliver 50% or less of the rainfall, with the other rain dominated by shorter-lived, isolated convective rain [*Fink et al.*, 2006; *Jackson et al.*, 2009]. An MCS is defined as a cloud system that produces a contiguous precipitation area on the order of 100 km or more in horizontal scale in at least one direction [American Meteorological Society, 2015]. MCSs grow and propagate through the action of mesoscale flows, particularly the cold pool, causing triggering of new convective cells all the time, therefore they are less sensitive to the patterns of local-scale convergence in their environment, and are more sensitive to the available moisture and CAPE [Corfidi, 2003]. Surface observations in the vicinity of Niamey [Taylor and Lebel, 1998] as well as idealized modeling of MCSs have shown how a pre-existing MCS will deliver more rainfall over a boundary layer with a higher specific humidity than its drier surrounding environment.

This therefore indicates two competing responses. Convective initiation is on the warm, dry side of boundaries and therefore local convection and the initial stages of MCS rain occur mostly in those areas, but mature MCS are thought to rain more over humid surfaces. This would indicate an additional feedback of the land surface state on the direction an MCS travels [Wolters et al., 2010]. If this is robust, then the net effect of the land surface on precipitation totals will depend on whether the climatology of a given zone is influenced by locally generated precipitation (small scale processes) or organized MCS precipitation (large scale processes).

Recent studies [*Taylor et al.*, 2013; *Birch et al.*, 2014] demonstrate that convection-permitting models provide a step change in the response of convection to the land surface which closely matches observations, even at relatively low spatial resolutions (12km). Convection-permitting models run over large domains therefore provide a valuable tool to evaluate the net effect of competing mechanisms that control the rainfall response to the surface. In this paper, we will examine the spatial coincidence of precipitation in relation to land cover from a high-resolution limited area simulation covering the entire West African monsoon region (approximately 3700km x 2400km), run with explicitly resolved convection. The combination of a high spatial resolution and a regional-scale domain allows us to explore, for the first time, mechanisms occurring across a range of scales in an integrated manner, in order to answer the following questions:

1. Location of rainfall
    a. Does convection initiate preferentially in the vicinity of forest-grass boundaries?
    b. Do MCS have a preference for moving over a certain land cover type?

2. Quantity of precipitation
    a. Is there more localised precipitation over boundaries?
    b. Does a mature MCS deliver more rain to different vegetation types within its swath?

Methodology

Numerical weather prediction model

The Met Office Unified Model [MetUM; *Davies et al.*, 2005] was used to create a dynamically downscaled 4 km resolution simulation similar to those described in [*Holloway et al.*, 2012]. The model is therefore configured in a similar way to that used for short-range weather prediction for the UK with, most notably, convection being represented explicitly. Furthermore, following [*Holloway et al.*, 2012], a 3-dimensional Smagorinsky-like [*Smagorinsky*, 1963] sub-grid turbulence scheme is employed, which replaces the 1-dimensional planetary boundary layer (PBL) parametrization scheme that would be used in coarser resolution simulations. This 3D sub-grid turbulence scheme governs the horizontal and vertical fluid flow via equations that account for sub-grid eddy viscosity and diffusivity. The classical Smagorinsky approach is extended by reducing the mixing length close to the surface in order to account for effects of the roughness of the land surface (a more detailed description of which can be found in [*Halliwell*, 2007; *Pearson et al.*, 2014]). The surface roughness length for momentum is calculated in the Joint UK Land Environment Simulator (JULES) land surface model as a multiple of PFT-dependent vegetation height (~28m for broadleaf tree and ~1.25m for C4 grass cover over the whole domain) and a PFT-specific ‘rate of change’ constant (0.05 for broadleaf tree, and 0.1 for C4 grass) that varies depending on plant functional type (PFT) [*Best et al.*, 2011]. Therefore the roughness lengths of broadleaf tree cover and C4 grass are 1.4m and 0.125m respectively. JULES also calculates heat and moisture fluxes to the PBL, thereby establishing a mechanistic link between the land surface properties and turbulence in the PBL. [*Holloway et al.*, 2012] have shown that the inclusion of the 3-dimensional sub-grid turbulence scheme can improve the simulation of tropical precipitation through the more realistic representation of turbulent flows.

This configuration involved running a 25km (n512 resolution) global forecast model, initialised with prescribed sea surface temperatures from OSTIA reanalyses [*Roberts-Jones et al.*, 2012], and ECMWF Integrated Forecast System soil moisture reanalyses [*Douville et al.*, 2000; *Drusch and Viterbo*, 2007]. The model simulation was run for the period 00:00 on 9th August 2006 to 24:00 on 19th August 2006, with the first 7 days rejected (following [*Birch et al.*, 2014]) to allow top layer soil moisture to reach equilibrium (further information on the soil moisture spinup is available in the supporting material), leaving the 4 day period from 00:00 on 16th August to 24:00 on 19th August for further analysis. Comparison of the 4 day period to satellite estimates if precipitation are discussed in the next section. Hourly lateral boundary conditions (LBCs) are generated from the global model using successive ECMWF operational analyses to create atmospheric conditions as close as possible to reality. The LBCs are then used to drive a 4km nested model (domain from 20.6°W to 12.6°E and 1.3°N to 22.9°N). The JULES land surface scheme [*Best et al.*, 2011] is used in the 4km model to characterise exchanges of heat, moisture and momentum between the land surface and the boundary layer. Vegetation is characterised as the fractional cover of 5 vegetated surface types (broadleaf tree, needleleaf tree, C3 grass, C4 grass, Shrub), and 4 non-vegetated surface types (Urban, Water, Bare Soil and Permanent Ice). Fractional cover of each surface type is derived from the IGBP Land Cover Classification [*Loveland and Belward*, 1997], with the cross walking conversion matrix described by [*Pacifico et al.*, 2011]. Transpiration from the vegetated surface types in JULES is dependent on a climatology of monthly varying leaf area index (LAI) derived from the MODIS sensor onboard the Terra satellite [*Knyazikhin et al.*, 1998; *Myneni et al.*, 2002], averaged over a 5 year period (2000 to 2004). In this simulation the LAI climatology for August was prescribed, to allow for seasonal differences in albedo, heat and moisture fluxes between natural grasslands and croplands.

Vegetation classification

In this study we used the land surface characteristics from the 4km limited area model as the basis for our analysis. Vegetation gradients were identified using the fractional cover of each land surface type, aggregated into 3 main classes: tree cover, grass cover, and sparse vegetation cover. Tree cover is defined where the tree fraction (sum of fractional cover of broadleaf tree, needleleaf tree and shrubs) was greater than 30%. Grass cover is the combination of both croplands and natural grasslands, and is defined where tree cover does not exist, and the grass fraction (sum of C3 and C4 grass cover) is greater than 30%. Sparse vegetation cover is defined where the tree and grass fractions are between 1% and 30%, and therefore bare soil fraction is greater than 70%. A 30% threshold of tree and shrub fraction to define forest cover, is chosen based on associations of direct airborne observations of the lower boundary layer to land cover classes [*Garcia-Carreras et al.*, 2010]. In this study, a linear transect over the northern part of Benin (9.7°N to 12.5°N), identified convergence zones in the planetary boundary layer that coincided with locations where vegetation transitioned from grass cover to shrub or tree fraction greater than 30%. Furthermore, comparison of surface evapotranspiration (from these simulations) with varying fractional tree and shrub cover (Figure S2) indicates that 30% tree and shrub cover fraction is a reasonable threshold to use for the definition of tree cover.

The boundaries between grass and tree cover were identified using a shifting 3x3 kernel (approximately 12km^2). If a kernel contained 3 or more grid cells of both grass and tree cover, it was identified as a boundary grid cell. The boundaries involving sparse vegetation cover were not considered in this analysis, as the evaporative fluxes from sparse vegetation were not considered sufficient to induce gradients in surface energy fluxes sufficient for the initiation of convection. Furthermore, the grass and tree sides of the boundary were defined as those grid cells within a 12km^2 buffer area around the boundary grid cells. Orographic effects on precipitation were discounted by excluding grid cells with an elevation greater than 500m from the analysis.

The study region chosen for further analysis was approximately located from 11°W to 10°E, and 4°N to 17°N (Figure 1). The study region was further sub-divided into 16 almost equal area zones, each measuring 4° x 4° in the model domain. These zones were chosen because they broadly represent the West

African biogeographical gradient from tropical forest in coastal areas (4.5°N to 8.5°N), to woody savannah (8.5°N to 12.5°N), to the sparsely vegetated arid Sahel region (12.5°N to 16.5°N). The zones were further subdivided longitudinally in order to aid the analysis of the incidence of precipitation over different cover types within similar locations.

Mesoscale convective system tracking algorithm

A tracking algorithm was adapted using the approach adopted by [*Mathon and Laurent*, 2001] to map MCS initiation, propagation and termination. The approach is based on simple overlaps between convective cells at 5 minute time steps [*Williams and Houze*, 1987]. Rather than using thresholds of cloud temperature, as a proxy for precipitation, to define MCS cells, we used modelled precipitation flux at 5 minute time intervals from the 4km simulations. We defined a precipitation cluster at a given 5 minute time step as a contiguous area of precipitation with rate greater than 1mm per hour. Precipitation clusters larger than 1000km^2 were defined as meso-scale convective systems, while clusters below this threshold were defined as localised precipitation. This approach is consistent with the approach by [*Mathon and Laurent*, 2001] in that there is no attempt to distinguish between the convective and stratiform parts of the MCS. The MCS size threshold of 1000 km^2 as opposed to 5000 km^2 used by [*Mathon and Laurent*, 2001]) reflects the smaller spatial occurrence of precipitation within a larger cloud cluster, as the wide cirrus shield provides a larger area in satellite outgoing long-wave radiation based detection. Following identification of MCS clusters, using the areal overlapping method we characterized 5 different stages of an MCS lifecycle. These included initiation, regular tracking, merging, splitting, and dissipation. The geometric centre point of the MCS, area, stage in life cycle and time, of each MCS was recorded at each time step, allowing further analysis. A more detailed description of each stage can be found in [*Mathon and Laurent*, 2001]. In order to relate the location at which convection first initiated to vegetation classes, precipitation clusters were tracked backwards from the point at which they first exceeded the 1000 km^2 threshold. A convection initiation point was therefore the location at which a contiguous area of precipitation at time t did not overlap with a cluster at time t-1. In many cases, one MCS could be related backwards to multiple initiation points. In order to remove the influence of pre-existing MCS on convective initiations via gravity waves or cold pools, initiations that merged with a larger convective cell within 30 minutes of the initiation time were disregarded.

Comparison to satellite estimates

Prior to using these simulations for analysis of the relationship between vegetation and precipitation, it is important to establish that the MetUM simulates the main features of precipitation dynamics for this period, such as the diurnal cycle of precipitation, African Easterly Wave (AEW) activity, and the propagation of precipitation. Estimates from the TRMM (Tropical Rainfall Measuring Mission) Multi-satellite Precipitation Analysis (TMPA; [*Huffman et al.*, 2007]) were compared to MetUM simulated precipitation for the 4 days of the simulation. Modelled 5 minute instantaneous precipitation rates were resampled to both the same spatial resolution (0.25 degrees) and the same temporal resolution (3 hourly accumulated precipitation) as the TMPA dataset. Figure 1(a) shows the east to west progression of precipitation across the domain during the 4 days of simulation, for both the MetUM and TMPA estimates. This shows that the MetUM captures the main periods of precipitation activity and in-activity that might be associated with AEWs. For example, the east-west propagation of precipitation observed by TMPA starting at approximately 18:00 on August 17th at 10°E, and ending at 12:00 on August 19th at 10°W was simulated by the MetUM in terms of approximate location and intensity. A similar period of precipitation activity occurs in TMPA from 12:00 on August 16th at 1°E, ending at 06:00 on August 17th at 10°E, where MetUM simulated precipitation is less spatially organised.

Figure 1(b) shows that the MetUM simulates well the diurnal cycle of precipitation with peaks in precipitation during the evening and night-time on each day similar to that of TMPA. The MetUM has a greater number of locations where precipitation is found (Figure 1a) compared to TMPA, which accounts for the higher rainfall totals found on August 18th to August 20th (Figure 1b). These differences are likely to be caused by the relatively infrequent 3 hourly observations of TMPA estimates compared to the 5 minute instantaneous precipitation output from the MetUM.

Location of rainfall

Does convection initiate preferentially in the vicinity of forest-grass boundaries? If so, when and where?

Understanding the contribution of vegetation gradients to the initiation of MCS in West Africa is important because of the large contribution of MCS to the total precipitation of the region [*Mathon et al.*, 2002]. Enhanced initiation of MCS has been shown over strong soil moisture gradients [*Taylor et al.*, 2011], and a mechanism for enhanced initiations over vegetation gradients has been identified using airborne measurements over savannah ecosystems [*Garcia-Carreras et al.*, 2011]. Understanding how the land surface interacts with the boundary layer during the monsoon period may furthermore elucidate the role of land use change in the local hydrological cycle. Here, we test the hypothesis, similar to the observational studies of [*Wang et al.*, 2009; *Knox et al.*, 2011], whether convection initiates preferentially over vegetation boundaries in a high resolution convection-permitting model.

To answer this question, we compared the points of convective initiation (PCI henceforth) to the land cover classes shown in Figure 2. Over the full 4 days of the simulation, 580 unique PCIs were recorded over land within the study domain (Table 1), which lead to the formation of 410 MCS in the study domain. In order to test the statistical significance of results, we formed a null hypothesis that the location of a PCI is not biased by land cover type, and that the expected probability of a PCI falling on a given land cover type is given by the fractional cover of that land cover type within the study domain. Assuming the data fit a binomial distribution, we estimate the uncertainty in the observed (from model simulations) number of PCIs for a given land cover class at the 90% confidence level, using a two-sided significance test [*R Core Team*, 2015]. Results are identified as significantly different than expected when the probability of obtaining the result by chance is less than 0.1.

For the afternoon period (13:00 to 18:00), we find significantly more than expected PCI over tree-grass boundaries, and less than expected PCI over tree cover (Table 1), indicating a positive bias of convective initiations towards the boundary class during the afternoon period. This equates to 19.0% (2.8% to 36.3%, at 90% confidence level) more convective initiations over boundaries than would be expected by chance. Similarly, we found a negative bias of PCI over tree cover in the afternoon, with 18.2% (1.2% to 33.5%) less PCI than expected by chance. The number of PCI for sparse vegetation, grass and orography classes was not significantly different from the expected. The reasons for these statistical differences are discussed further in the next section.

For all times of day, we find significantly fewer than expected PCI over grass cover, and significantly more PCI over orography, indicating a general positive bias towards orography and a negative bias towards grass cover. The number of PCIs over boundary, tree and sparse cover were within the expected range for those land cover classes. As shown in Figure 3, convective initiations tend to occur more frequently during the period 13:00 to 18:00. During these 5 hours, 49% of all convective initiations occur, with the majority of PCIs occurring over grass and boundary classes (191 out of 284). During this period, 33.8% of all convective initiations occurred over boundary cover, more than would be expected by chance at the 90% confidence level.

The spatial and temporal distribution of convective initiations in the simulations reveals further patterns related to land cover. Figure 2 shows that PCIs are generally located in 3 main areas: the savannah regions of Togo and Ghana (6N to 11N; 3W to 5E); from the forest belt extending from central Nigeria to Eastern Burkina Faso (7N to 12N; 1E to 5E); and the fragmented forests of Cote d'Ivoire and Liberia northwards into Western Burkina Faso (5N to 12N; 11W to 3W). In general terms, each of these three areas coincide with either the edges of larger forest patches or many smaller patches of forest. Afternoon initiations do appear to be clustered around tree-grass boundaries in many areas, providing visual evidence to support the statistics for the whole study area presented in Table 1.

Convective initiations, however, do not follow the same spatial and temporal patterns each day. Figure 4 shows how the locations of PCI vary according to time and location during the simulation. During the afternoon of August 16th, there are very high numbers of convective initiations south of 13N, which occur either on (0-5km distance) or very near to boundaries (5-10km). Within this period, clusters of convective initiations on boundaries can be seen between 7W to 3W (triangles) and 6N to 8N between 12:00 and 15:00, coinciding with the grass-forest boundaries in southern and northern Cote d'Ivoire. Similar afternoon activity is also seen in central Ghana (7N to 8N) and northern Benin (11N to 12N). In contrast to subsequent days, on August 16th very little PCI occurs north of 12N, and the little that does occur is at least 10-20km from a vegetation boundary. The following day, August 17th, has a very different spatial pattern of convective initiations, and generally reduced afternoon activity. Approximately half of all PCIs occur north of 12N, which is much further north than the previous day, and a long distance from a boundary (between 12:00 and 15:00). The boundary initiations that do occur on August 17th occur later (15:00 to 18:00), albeit in similar locations to the previous day (South Central Ghana, and northern Cote d'Ivoire). August 18th again has convective initiations distributed across all the latitudes within the study region, but PCI are more clustered towards the south east (South Nigeria) and north east (South Niger) of the study region, albeit with some afternoon PCI again over boundaries in North Cote d'Ivoire. The fourth day of the simulation (August 19th) shows a return to afternoon initiations occurring south of 12N, similar to August 16th, with afternoon PCI occurring mostly over South and Central Nigeria, and North Ghana. These differences, in particular the similarity of spatial pattern during August 16th to August 19th indicates that the land surface requires a period of recovery following a rainfall event. Direct observations of surface fluxes acquired during the African Monsoon Multidisciplinary Analysis (AMMA) by [*Lohou et al.*, 2014] show that the land surface response to rainfall events varies considerably depending on the vegetation type. Here, the length of the recovery period was found to range from 1 day for bare soil, to up to 70 days for tree cover. Over the Hombori grassland site in Mali (15.5°N, 1.5°E), recovery time was found to be approximately 4 days after the rainfall event.

Why does convection initiate preferentially over boundaries?

To understand what is causing these variations in convective initiations, we extracted model diagnostics for u and v 10m wind components, 1.5m specific humidity (*sh*), land surface temperature (*lst*), and bowen ratio (*br*). For each afternoon PCI (between 13:00 and 18:00), we extracted these values for a 1°x1° box centred on the PCI 90 minutes before the time of convective initiation (t_{-90}) in order to capture the surface conditions prior to the initiation of convection. Using the U and V wind components, we calculated the modal wind direction at t-

$_{90}$, and rotated the corresponding *sh*, *lst* and *br* to the direction of the prevailing wind, such that grid cells north of the centre point show the surface conditions directly upwind. Each rotated 1°x1° box was then averaged to provide the mean surface conditions in relation to the prevailing wind direction.

The results in Figure 5 show that when a PCI occurs over boundary cover in zones 7, 8 and 9 during the afternoon, there is predominantly more tree cover upwind and more grass cover downwind. This distribution of vegetation cover is directly associated with higher *sh* and lower *lst* upwind, compared to lower *sh* and higher *lst* downwind. Furthermore, this is also reflected in the strong gradient of *br* at the point of convective initiation over the boundary, indicating a vegetation boundary-induced convergence of heat and moisture in the savannah region of West Africa. These results extend the findings of [*Marsham et al.*, 2013; *Birch et al.*, 2014] who identified pressure gradients in explicit convection simulations that were modified by moist convective heating during the daytime period. Here, we show that such moist heating gradients can be related to vegetation gradients in the central zone of West Africa (9N to 13N).

Do MCS have a preference for moving over a certain land cover type, at different times of day?

We pose this question because as convective cells grow and begin to propagate, it would be expected that their path, as well as the intensity of rainfall within them, are affected by both the supply of moisture, and convergence along strong thermal gradients induced by surface heterogeneity as hypothesised by [*Anthes*, 1984]. As precipitation falls from the MCS along a squall line, cold air propagates away from the MCS in a cold-pool, and convergence occurs at the interface between this cool air and warmer ambient air, triggering new convective cells in the system. It might be expected that MCS precipitation occurs more readily over vegetation types which favour a high level of energy on which convective cells can feed – that is, high column moisture and high CAPE. Two case-study modelling papers [*Schwendike et al.*, 2010; *Wolters et al.*, 2010] have shown that MCS tracks preferentially move towards regions with high available moisture and energy for the storm, indicating a positive feedback of soil moisture. However, there has been no systematic study of this process, and it remains uncertain.

Here, in order to understand whether precipitation statistics from the simulations support this hypothesis, we plot the total amount of time MCS precipitation occurs over land cover classes within the zones identified in Figure 1, normalized by the total area of that land cover class within the zone. The normalization removes any bias towards the quantity of land cover within a zone. Assuming no preference for any vegetation type, we would expect mean MCS time to be equal for all land cover types within a zone, with variation between zones indicating geographical differences in the MCS time.

We can see from Figure 6a that there is a strong orographic effect on the average amount of time MCS precipitation occurs over a land cover class, especially in zones 5, 6, 10 and 11, where the majority of orography occurs in the study region. Given the short timescale of the simulations and the latitudinal position of the inter-tropical convergence zone, we choose to focus on the zones with the highest quantity of afternoon-evening precipitation and little or no orographic influence (zones 7, 8 and 9). We find that in zone 7, on average 9 minutes more MCS time is spent over boundary than over tree cover. In zone 8, this reduces to 4-5 minutes more MCS time over boundary cover, whereas in zone 9, on average 4 minutes more MCS time is spent over tree cover.

Quantity of precipitation

Is there more localised precipitation over boundaries?

Given that in some zones of the region, and in other parts of the world, the total rainfall is dominated by isolated, rather than MCS rainfall, we also examined the occurrence of small-scale (area < $1000 km^2$) precipitation in relation to vegetation classes. We hypothesise that small-scale precipitation falls preferentially over certain land cover types during the afternoon period (15:00 to 21:00). Accumulated precipitation for each land cover type and zone during the afternoon period for all 4 days of the simulations is multiplied by the fraction of that land cover type within a given zone. This gives a normalised quantity, which can be used to compare amounts of precipitation accumulation between different cover types within a zone. Therefore, figure 7a provides an indication of whether small-scale precipitation falls preferentially over different cover types in different parts of the study area.

Figure 7a shows that more afternoon small-scale precipitation occurs over grass cover than any other vegetated cover types in zones 7, 8, 10, 11 and 12. Large amounts of precipitation over orography are also found in zones 6, 10 and 11, the areas with the largest amount of land over 500m above sea level. A clear preference of small-scale precipitation towards a particular vegetation type is more difficult to discern in locations where little afternoon small-scale precipitation occurs (zones 1 to 5), where there is a large coastal fraction (zones 11 to 15), or where large amounts of orography occur (zones 5, 6, 10 and 11).

Does a mature MCS deliver more rain to different vegetation types within its swath?

While subjective measures of where MCS travel are possible from these simulations, it is not possible to say whether vegetation has influenced the location of MCS tracks. However, within an MCS swath that covers grass boundary and tree simultaneously, it is possible to test over which cover type the most intense part of the MCS precipitation falls. We compare mean precipitation rates within the convective part (>10mm) of an MCS (Table 2) only in cases where the MCS covers more than 10% of all three land cover classes (tree, grass or boundary). For each MCS at each 5-minute time step where the 10% criteria was met, the class with the greatest mean intense precipitation was recorded. All other things being equal, we would expect an equal probability (one third) of one land cover class being greater than the other two. However, we find a clear preference towards tree cover, with 48.4% of times that an MCS occurred over all three cover types, the mean rate of convective precipitation was greatest over tree cover. This preference for intense precipitation over tree cover was found to occur in both early morning periods (01:00 to 07:00) and in the afternoon to evening period (13:00 to 19:00). The inverse was found for boundary cover, where the most intense precipitation within an MCS was found to occur only 19.9% of times over this cover type at all times of day ($p<0.1$).

Discussion

These results show that convective initiations do occur more frequently over tree-grass boundaries during the afternoon in the simulations, particularly in the central parts of the study domain (zones 7, 8 and 9 between 9°N to 13°N and 7°W to 5°E). The mechanism for convective initiations over tree-grass boundaries is shown to be related to strong horizontal gradients of heat and moisture in the upwind direction, associated with vegetation gradients. This is indicated by higher specific humidity, lower land surface temperature, and more frequent tree cover upwind of points of convective initiation. Downwind of convective initiations, we found a greater frequency of grass cover, associated with higher land surface temperatures and lower specific humidity. The gradient of convective heating on the vegetation boundary is further diagnosed in these simulations by the strong upwind gradient of the bowen ratio at the point of convective initiation. This means that the physical mechanism driving the results shown here is directly comparable to the results shown by observational studies of vegetation and soil moisture induced convective initiations [*Shaw and Doran*, 2001; *Garcia-Carreras et al.*, 2010; *Taylor et al.*, 2011], where upwind gradients of bowen ratio were identified as drivers of convective initiations. This is also in alignment with other modelling studies using large eddy simulations of turbulent boundary layer flows. For example, [*Letzel and Raasch*, 2003; *Garcia-Carreras et al.*, 2011; *Kang and Bryan*, 2011] describe in more detail how convection initiates over heterogeneous land surfaces by alternating warm-dry conditions with cool-moist conditions at a variety length scales from 2.5km to 200kms.

Statistically, we found that 33.8% (29.2% to 38.7%; $p < 0.1$) of all afternoon initiations occur over forest-grass boundaries that occupy 28.4% of the land surface in the study area, showing that more initiations occur over forest-grass boundaries than would be expected by chance. This represents a similar effect to that observed from soil moisture by [*Taylor et al.*, 2011], where 37% of all MCS initiations were discovered over the steepest 25% of the soil moisture gradients. This also supports the findings of [*Garcia-Carreras et al.*, 2010] who used aircraft observations over Benin to relate mesoscale convergence patterns to gradients of vegetation cover. [*Garcia-Carreras et al.*, 2010] also showed that this mesoscale organisation was attributed to variability in sensible heat flux at boundaries between tree/shrub cover and croplands.

Furthermore, once convection initiates, these results show that rainfall totals from small-scale precipitation tend to favour grass cover (Figure 7). This would indicate that while convective initiations occur over tree-grass boundaries, small-scale convection tends to move towards the warm, dry side of vegetation boundaries in the period between 15:00 and 21:00. This was found in zones 7, 8, 10, 11 and 12, where the majority of MCS initiations also occur, which would fit with observations of more afternoon rain over dry soils in semi-arid regions [*Taylor et al.*, 2012]. A similar preference of tropical rainfall for the warm, dry side of tree-crop boundaries was found over the southwestern Amazon by [*Knox et al.*, 2011], using satellite-borne precipitation radar observations. A recent study by [*Mande et al.*, 2015] however contradicts this finding when comparing savannah woodland and agricultural land sites separated by only 1.5km. This contradiction indicates that perhaps the 4km grid length of these MetUM simulations is not sufficient to fully characterise land surface interactions with the boundary layer. Observational studies have shown that these convective events can have a significant contribution to local scale Sahelian precipitation variability [*D'amato and Lebel*, 1998; *Taylor and Lebel*, 1998] and regional scale precipitation totals [*Mathon and Laurent*, 2001] as convection initiated on boundaries grows and begins to organise into larger MCS.

The average amount of time an MCS occurs over different cover types shows a less clear pattern in these simulations (Figure 6) during the afternoon and evening period (15:00 to 21:00). On average during this period of the day, MCS spend a greater proportion of time over orography in zones with a high fraction of orography (zones 6 and 10 covering the Guinea Highlands and zone 11 covering the Jos Plateau). It would be reasonable to expect that the locations where vegetation may influence an MCS to be where MCS are most commonly found (zones 7, 8 and 9), but not influenced by close proximity to the sea (zones 11 to 15) and not influenced by orography (zones 6, 10 and 11). However, zones 7, 8 and 9 don't reveal a consistent pattern in terms of the time an MCS spends over each cover type. While zone 7 shows MCS spend more time over tree-grass boundaries, zone 9 shows MCS spend more time over tree cover. This inconsistency may be due to the short timespan of the simulations not allowing sufficient time to create robust statistics, or equally it may be due to the locations at which convection initiations occur, the general direction of regional scale circulation, and the speed of MCS travel. For example, if more convective initiations than expected occur over the Jos Plateau in zone 10 during the early afternoon, the speed of travel and direction of large-scale circulation (east to west) may result in more MCS than expected over the forest area of zone 9.

However, looking at the region as a whole, we find a preference for the most intense part of MCS precipitation to be situated over tree cover (Table 2), when the MCS covers tree, grass and boundary simultaneously. This would support the theory that MCS precipitation falls most intensely on surfaces with a strong supply of moisture, and that tree cover provides a similar feedback mechanism to that of soil moisture as shown by [*Wolters et al.*, 2010]. However, in order to further investigate this feedback mechanism in the MetUM, more extensive idealised experiments would need to be conducted similar to [*Lauwaet et al.*, 2010].

Subjectively, the largest MCS found during the afternoon or evening period appear to track tree cover or tree-grass boundary areas (not shown), however, objective measures of whether an MCS moves towards certain cover types were not possible in this simulation. This may be due to the highly heterogeneous landscapes found under these large convective complexes, and the relative insensitivity of MCS to small-scale features of the land surface. It should also be noted that the spatial coincidence of MCS and tree cover is not an indication of a feedback response. Indeed, tree cover may persist more readily where, climatologically, MCS tracks occur most frequently. One might also consider that MCS occur over grass by chance in the afternoon to evening period. For example, if MCS are more likely to initiate over orography to the north and east of the domain, given the speed and direction at which they generally travel it might be expected that they reach the area of tree-grass boundaries found in Benin, Burkina Faso and Cote d'Ivoire, or the large area of grass cover in central and northern Ghana.

The evidence from this modelling experiment points towards different feedback responses in different parts of West Africa, at different spatial scales. This may firstly be due to precipitation being sensitive to different fractions of tree cover at different latitudes. For example, Figure 5a shows that more small scale precipitation than expected falls over tree cover or tree-grass boundaries in Sahelian zones (3 and 4), whereas further south, in savannah zones (7 and 8), more small scale precipitation than expected falls over grass cover. Secondly, the influence of the land surface on MCS propagation and intensity is likely to change at different times of day, the strength of which may also depend on large scale circulation.

Conclusions

We show that in convection-permitting high resolution simulations of the West African monsoon, significantly more convective initiations occur over tree-grass boundaries than would be expected by the surface area of vegetation boundaries. The vegetation feedback in the simulations is of a similar magnitude to the feedback observed from soil moisture by [*Taylor et al.*, 2011]. The mechanism for this feedback has been shown to be due to gradients of heat and moisture induced by the upwind tree cover (cooler, more moist air) and downwind grass cover (warmer, drier air). Furthermore, when an MCS simultaneously covers grass, boundary and tree cover, the most intense precipitation was found to occur over forest cover 48.4% of the time, indicating that the moisture supplied by tree cover provides a positive feedback to precipitation.

These results therefore show that convection-permitting NWP models are suitable tools for simulating the response of convective precipitation to changes in land cover. This is particularly relevant to issues related to land use planning in the context of water and forest management in arid and semi-arid areas that are prone to sustained periods of drought.

References

American Meteorological Society (2015), Mesoscale Convective System, *Am. Meteorol. Soc.*

Anthes, R. A. (1984), Enhancement of Convective Precipitation by Mesoscale Variations in Vegetative Covering in Semiarid Regions, *J. Clim. Appl.*

Meteorol., *23*(4), 541–554, doi:10.1175/1520-0450(1984)023<0541:EOCPBM>2.0.CO;2.

Best, M. J. et al. (2011), The Joint UK Land Environment Simulator (JULES), model description – Part 1: Energy and water fluxes, *Geosci. Model Dev.*, *4*(3), 677–699, doi:10.5194/gmd-4-677-2011.

Birch, C. E., D. J. Parker, J. H. Marsham, D. Copsey, and L. Garcia-Carreras (2014), A seamless assessment of the role of convection in the water cycle of the West African Monsoon, *J. Geophys. Res. Atmos.*, *119*(6), 2890–2912, doi:10.1002/2013JD020887.

Corfidi, S. F. (2003), Cold Pools and MCS Propagation: Forecasting the Motion of Downwind-Developing MCSs, *Weather Forecast.*, *18*(6), 997–1017, doi:10.1175/1520-0434(2003)018<0997:CPAMPF>2.0.CO;2.

D'amato, N., and T. Lebel (1998), On the characteristics of the rainfall events in the Sahel with a view to the analysis of climatic variability, *Int. J. Climatol.*, *18*, 955–974, doi:10.1002/(SICI)1097-0088(199807)18:9<955::AID-JOC236>3.0.CO;2-6.

Davies, T., M. J. P. Cullen, A. J. Malcolm, M. H. Mawson, a. Staniforth, A. A. White, and N. Wood (2005), A new dynamical core for the Met Office's global and regional modelling of the atmosphere, *Q. J. R. Meteorol. Soc.*, *131*(608), 1759–1782, doi:10.1256/qj.04.101.

Douville, H., P. Viterbo, J.-F. Mahfouf, and A. C. M. Beljaars (2000), Evaluation of the Optimum Interpolation and Nudging Techniques for Soil Moisture Analysis Using FIFE Data, *Mon. Weather Rev.*, *128*(6), 1733–1756, doi:10.1175/1520-0493(2000)128<1733:EOTOIA>2.0.CO;2.

Drusch, M., and P. Viterbo (2007), Assimilation of Screen-Level Variables in ECMWF's Integrated Forecast System: A Study on the Impact on the Forecast Quality and Analyzed Soil Moisture, *Mon. Weather Rev.*, *135*(2), 300–314, doi:10.1175/MWR3309.1.

Fink, A. H., D. G. Vincent, and V. Ermert (2006), Rainfall Types in the West African Sudanian Zone during the Summer Monsoon 2002, *Mon. Weather Rev.*, *134*(8), 2143–2164, doi:10.1175/MWR3182.1.

Garcia-Carreras, L., and D. J. Parker (2011), How does local tropical deforestation affect rainfall?, *Geophys. Res. Lett.*, *38*(19), L19802, doi:10.1029/2011GL049099.

Garcia-Carreras, L., D. J. Parker, C. M. Taylor, C. E. Reeves, and J. G. Murphy (2010), Impact of mesoscale vegetation heterogeneities on the dynamical and thermodynamic properties of the planetary boundary layer, *J. Geophys. Res.*, *115*(D3), D03102, doi:10.1029/2009JD012811.

Garcia-Carreras, L., D. J. Parker, and J. H. Marsham (2011), What is the Mechanism for the Modification of Convective Cloud Distributions by Land Surface–Induced Flows?, *J. Atmos. Sci.*, *68*(3), 619–634, doi:10.1175/2010JAS3604.1.

Halliwell, C. (2007), *Subgrid turbulence schemeHalliwell C. 2007. "Subgrid* *turbulence scheme",UnifiedModel Documentation Paper 28. Met Office: Exeter, UK.*, UnifiedModel Documentation Paper, Exeter, UK.

Hansen, M. C. et al. (2013), High-Resolution Global Maps of 21st-Century Forest Cover Change, *Science (80-.).*, *342*(6160), 850–853, doi:10.1126/science.1244693.

Holloway, C. E., S. J. Woolnough, and G. M. S. Lister (2012), Precipitation distributions for explicit versus parametrized convection in a large-domain high-resolution tropical case study, *Q. J. R. Meteorol. Soc.*, *138*(668), 1692–1708, doi:10.1002/qj.1903.

Huffman, G. J., D. T. Bolvin, E. J. Nelkin, D. B. Wolff, R. F. Adler, G. Gu, Y. Hong, K. P. Bowman, and E. F. Stocker (2007), The TRMM Multisatellite Precipitation Analysis (TMPA): Quasi-Global, Multiyear, Combined-Sensor Precipitation Estimates at Fine Scales, *J. Hydrometeorol.*, *8*(1), 38–55, doi:10.1175/JHM560.1.

Jackson, B., S. E. Nicholson, and D. Klotter (2009), Mesoscale Convective Systems over Western Equatorial Africa and Their Relationship to Large-Scale Circulation, *Mon. Weather Rev.*, *137*(4), 1272–1294, doi:10.1175/2008MWR2525.1.

Kang, S.-L., and G. H. Bryan (2011), A Large-Eddy Simulation Study of Moist Convection Initiation over Heterogeneous Surface Fluxes, *Mon. Weather Rev.*, *139*(9), 2901–2917, doi:10.1175/MWR-D-10-05037.1.

Knox, R., G. Bisht, J. Wang, and R. Bras (2011), Precipitation Variability over the Forest-to-Nonforest Transition in Southwestern Amazonia, *J. Clim.*, *24*(9), 2368–2377, doi:10.1175/2010JCLI3815.1.

Knyazikhin, Y., J. V. Martonchik, R. B. Myneni, D. J. Diner, and S. W. Running (1998), Synergistic algorithm for estimating vegetation canopy leaf area index and fraction of absorbed photosynthetically active radiation from MODIS and MISR data, *J. Geophys. Res.*, *103*(D24), 32257, doi:10.1029/98JD02462.

Lauwaet, D., N. P. M. Lipzig, N. Kalthoff, and K. Ridder (2010), Impact of vegetation changes on a mesoscale convective system in West Africa, *Meteorol. Atmos. Phys.*, *107*(3-4), 109–122, doi:10.1007/s00703-010-0079-7.

Letzel, M. O., and S. Raasch (2003), Large Eddy Simulation of Thermally Induced Oscillations in the Convective Boundary Layer, *J. Atmos. Sci.*, *60*(18), 2328–2341, doi:10.1175/1520-0469(2003)060<2328:LESOTI>2.0.CO;2.

Lohou, F. et al. (2014), Surface response to rain events throughout the West African monsoon, *Atmos. Chem. Phys.*, *14*(8), 3883–3898, doi:10.5194/acp-14-3883-2014.

Loveland, T. R., and A. S. Belward (1997), The IGBP-DIS global 1km land cover data set, DISCover: First results, *Int. J. Remote Sens.*, *18*(15), 3289–3295, doi:10.1080/014311697217099.

Mahmood, R. et al. (2014), Land cover changes and their biogeophysical effects on climate, *Int. J. Climatol.*, *34*(June 2013), 929–953, doi:10.1002/joc.3736.

Mande, T., N. C. Ceperley, G. G. Katul, S. W. Tyler, H. Yacouba, and M. B. Parlange (2015), Suppressed convective rainfall by agricultural expansion in southeastern Burkina Faso, *Water Resour. Res.*, *51*(7), 5521–5530, doi:10.1002/2015WR017144.

Marsham, J. H., N. S. Dixon, L. Garcia-Carreras, G. M. S. Lister, D. J. Parker, P. Knippertz, and C. E. Birch (2013), The role of moist convection in the West African monsoon system: Insights from continental-scale convection-permitting simulations, *Geophys. Res. Lett.*, *40*(9), 1843–1849, doi:10.1002/grl.50347.

Mathon, V., and H. Laurent (2001), Life cycle of Sahelian mesoscale convective cloud systems, *Q. J. R. Meteorol. Soc.*, *127*(572), 377–406, doi:10.1002/qj.49712757208.

Mathon, V., H. Laurent, and T. Lebel (2002), Mesoscale Convective System Rainfall in the Sahel, *J. Appl. Meteorol.*, *41*(11), 1081–1092, doi:10.1175/1520-0450(2002)041<1081:MCSRIT>2.0.CO;2.

Myneni, R. . et al. (2002), Global products of vegetation leaf area and fraction absorbed PAR from year one of MODIS data, *Remote Sens. Environ.*, *83*(1-2), 214–231, doi:10.1016/S0034-4257(02)00074-3.

Pacifico, F. et al. (2011), Evaluation of a photosynthesis-based biogenic isoprene emission scheme in JULES and simulation of isoprene emissions under present-day climate conditions, *Atmos. Chem. Phys.*, *11*(9), 4371–4389, doi:doi:10.5194/acp-11-4371-2011.

Pearson, K. J., G. M. S. Lister, C. E. Birch, R. P. Allan, R. J. Hogan, and S. J. Woolnough (2014), Modelling the diurnal cycle of tropical convection across the “grey zone,” *Q. J. R. Meteorol. Soc.*, *140*(679), 491–499, doi:10.1002/qj.2145.

R Core Team (2015), R: A language and environment for statistical computing,

Roberts-Jones, J., E. K. Fiedler, and M. J. Martin (2012), Daily, Global, High-Resolution SST and Sea Ice Reanalysis for 1985–2007 Using the OSTIA System,

Schwendike, J., N. Kalthoff, and M. Kohler (2010), The impact of mesoscale convective systems on the surface and boundary-layer structure in West Africa: Case-studies from the AMMA campaign 2006, *Q. J. R. Meteorol. Soc.*, n/a–n/a, doi:10.1002/qj.599.

Segal, M., and R. W. Arritt (1992), Nonclassical Mesoscale Circulations Caused by Surface Sensible Heat-Flux Gradients, *Bull. Am. Meteorol. Soc.*, *73*(10), 1593–1604, doi:10.1175/1520-0477(1992)073<1593:NMCCBS>2.0.CO;2.

Shaw, W. J., and J. C. Doran (2001), Observations of Systematic Boundary Layer Divergence Patterns and Their Relationship to Land Use and Topography, *J. Clim.*, *14*(8), 1753–1764, doi:10.1175/1520-0442(2001)014<1753:OOSBLD>2.0.CO;2.

Smagorinsky, J. (1963), General circulation experiments with the primitive equations, *Mon. Weather Rev.*, *91*(3), 99–164, doi:10.1175/1520-0493(1963)091<0099:GCEWTP>2.3.CO;2.

Taylor, C. M., and T. Lebel (1998), Observational Evidence of Persistent Convective-Scale Rainfall Patterns, *Mon. Weather Rev.*, *126*(6), 1597–1607, doi:10.1175/1520-0493(1998)126<1597:OEOPCS>2.0.CO;2.

Taylor, C. M., A. Gounou, F. Guichard, P. P. Harris, R. J. Ellis, F. Couvreux, and M. De Kauwe (2011), Frequency of Sahelian storm initiation enhanced over mesoscale soil-moisture patterns, *Nat. Geosci.*, *4*(7), 430–433, doi:10.1038/ngeo1173.

Taylor, C. M., R. a M. de Jeu, F. Guichard, P. P. Harris, and W. a Dorigo (2012), Afternoon rain more likely over drier soils., *Nature*, *489*(7416), 423–6, doi:10.1038/nature11377.

Taylor, C. M., C. E. Birch, D. J. Parker, N. Dixon, F. Guichard, G. Nikulin, and G. M. S. Lister (2013), Modeling soil moisture-precipitation feedback in the Sahel: Importance of spatial scale versus convective parameterization, *Geophys. Res. Lett.*, *40*(23), 6213–6218, doi:10.1002/2013GL058511.

Wang, J., F. J. F. Chagnon, E. R. Williams, A. K. Betts, N. O. Renno, L. A. T. Machado, G. Bisht, R. Knox, and R. L. Bras (2009), Impact of deforestation in the Amazon basin on cloud climatology., *Proc. Natl. Acad. Sci. U. S. A.*, *106*(10), 3670–4, doi:10.1073/pnas.0810156106.

Williams, M., and R. A. Houze (1987), Satellite-Observed Characteristics of Winter Monsoon Cloud Clusters, *Mon. Weather Rev.*, *115*(2), 505–519, doi:10.1175/1520-0493(1987)115<0505:SOCOWM>2.0.CO;2.

Wolters, D., C. C. van Heerwaarden, J. V.-G. de Arellano, B. Cappelaere, and D. Ramier (2010), Effects of soil moisture gradients on the path and the intensity of a West African squall line, *Q. J. R. Meteorol. Soc.*, *136*(653), 2162–2175, doi:10.1002/qj.712.

Tables

Table 1 Number and percentage of convective initiations by land cover type during the full 4-day period for all times of day, and for the afternoon period (13:00 to 18:00). The total land area and percentage cover of each surface type shows the expected proportion of convective initiations if land cover had no influence on the location of convective initiations. Asterisks denote significant results ($p < 0.1$) according to a two-tailed binomial test, with a null hypothesis that the observed percentage of convective initiations (from model simulations) over a land cover class is equal to the expected proportion. Uncertainty in the observed percentage of convective initiations by vegetation type is shown using the lower and upper 90% confidence interval from the significance test.

Land cover type	**Land Area**		**Convective initiations All times of day**		**Convective initiations Afternoon**	
	Km^2	%	n	lower % upper	n	lower % upper
Sparse	126,459	4.6	18	2.0 3.1 4.6	10	1.9 3.5 5.9
Grass	956,306	34.9	172	26.5 29.7* 32.9	95	28.8 33.5 38.3
Boundary	778,532	28.4	173	26.7 29.8 33.1	96	29.2 33.8* 38.7
Tree	696,185	25.4	145	22.1 25.0 28.1	59	16.9 20.8* 25.1
Orography	181,131	6.6	72	10.2 12.4* 14.9	24	5.9 8.5 11.7
Total	2,738,630	100	580	100	284	100

Table 2 Probability of mean intense rainfall being greater over one cover type than another, where precipitation occurs over all 3 cover types simultaneously, within the MCS. Assuming that there is no preference for a particular cover type, all probabilities would be expected to be 0.33. For example, in cases where MCS precipitation occurred over tree (t), grass (g) and boundary (b) cover at the same time, in 48.4% of cases the most intense rainfall was over the tree cover rather than grass or boundary cover. Asterisks indicate significant results (p<-0.1) under a two-tailed binomial test.

	All day % (lower % upper) n=413	01:00 to 07:00 (lower % upper) n=214	13:00 to 19:00 (lower % upper) n=92
$P(t > g \cup t > b)$	48.4* (43.6 to 53.2)	49.5* (42.9 to 56.2)	43.5* (33.8 to 53.7)
$P(g > t \cup g > b)$	31.7 (27.4 to 36.4)	30.8 (25.0 to 37.3)	34.8 (25.8 to 44.9)
$P(b > t \cup b > g)$	19.9* (16.3 to 24.0)	19.6* (14.9 to 25.5)	21.7* (14.5 to 31.2)

Figures

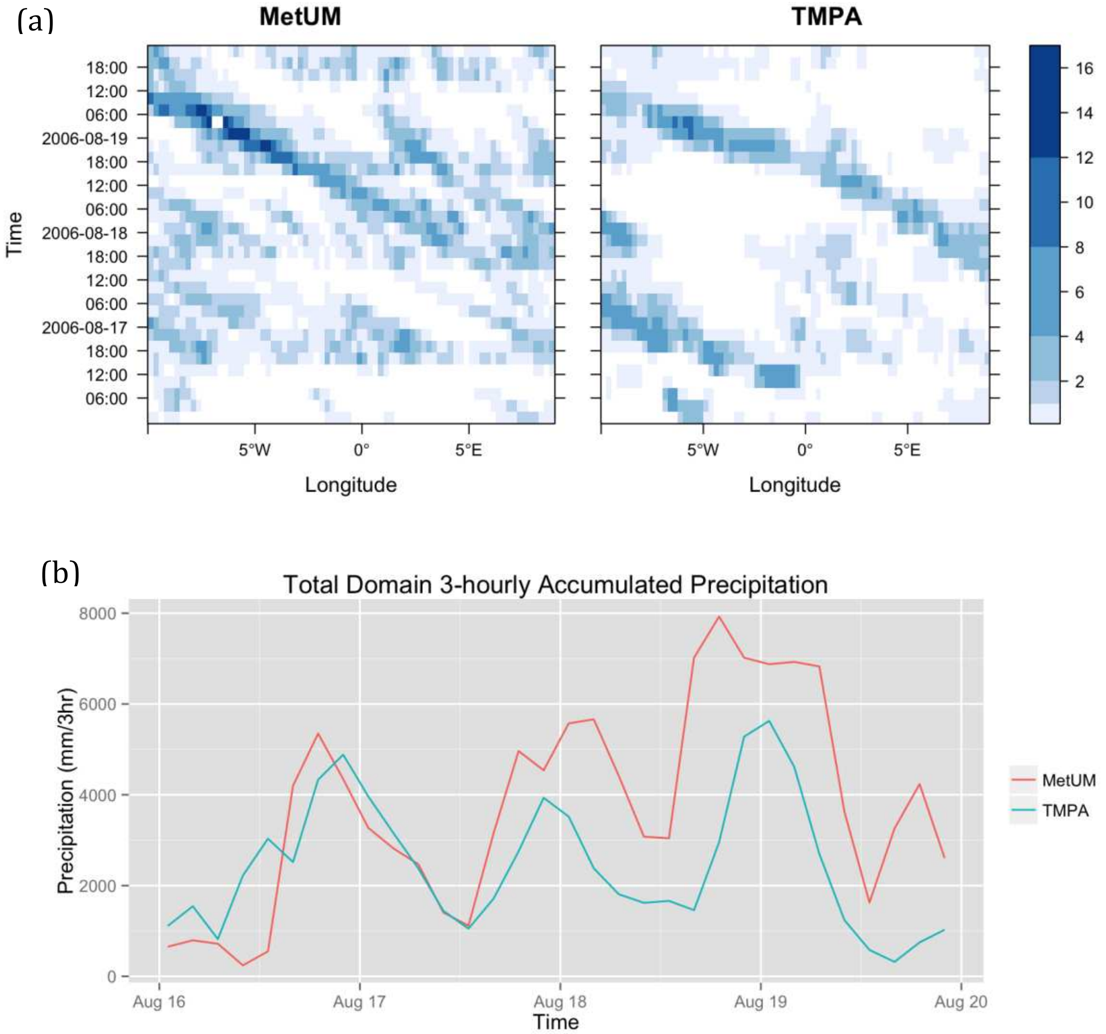

Figure 1 Hovmoller plots (a) of MetUM and TRMM satellite estimates for 3-hourly accumulated precipitation (mm/3hr). Each grid cell shows mean accumulated precipitation between 5°N and 17°N for each 0.25° longitude increment at 3-hourly time steps. Total 3-hourly accumulated precipitation (b) is shown for the full domain (11°W to 9°E and 5°N to 17°N).

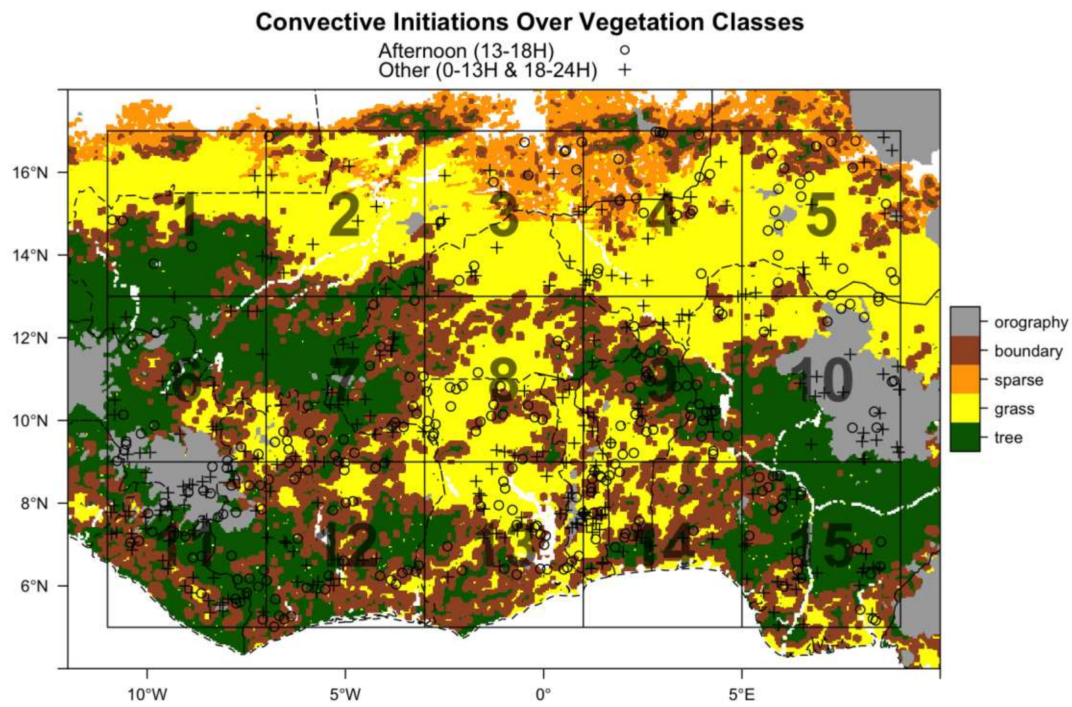

Figure 2 Vegetation classes and numbered zones (referred to in subsequent figures). Grey areas represent regions with an elevation greater than 500m, which were excluded from the analysis. Points indicate convective initiations split between afternoon initiations (13:00 to 18:00; open circles) and all other times (0:00 to 13:00 and 18:00 to 24:00; crosses), overlaid on vegetation classes. Terrestrial water bodies, shown in white, were excluded from the analysis.

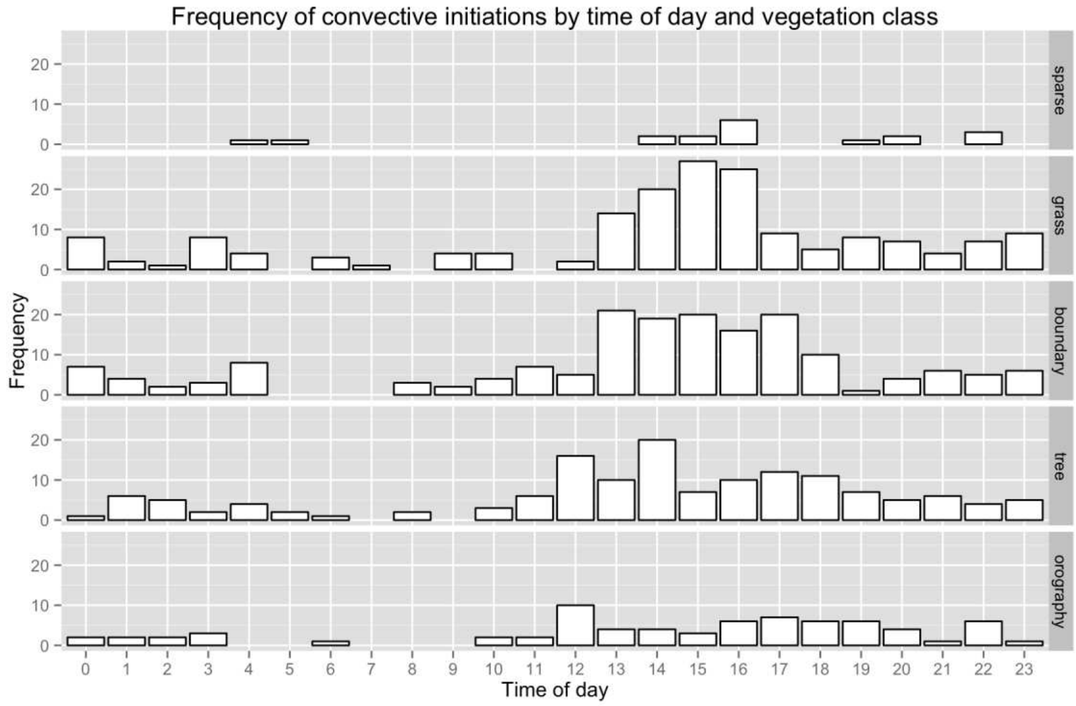

Figure 3 Total number of convective initiations for the 4-day simulations by time of day and land cover class.

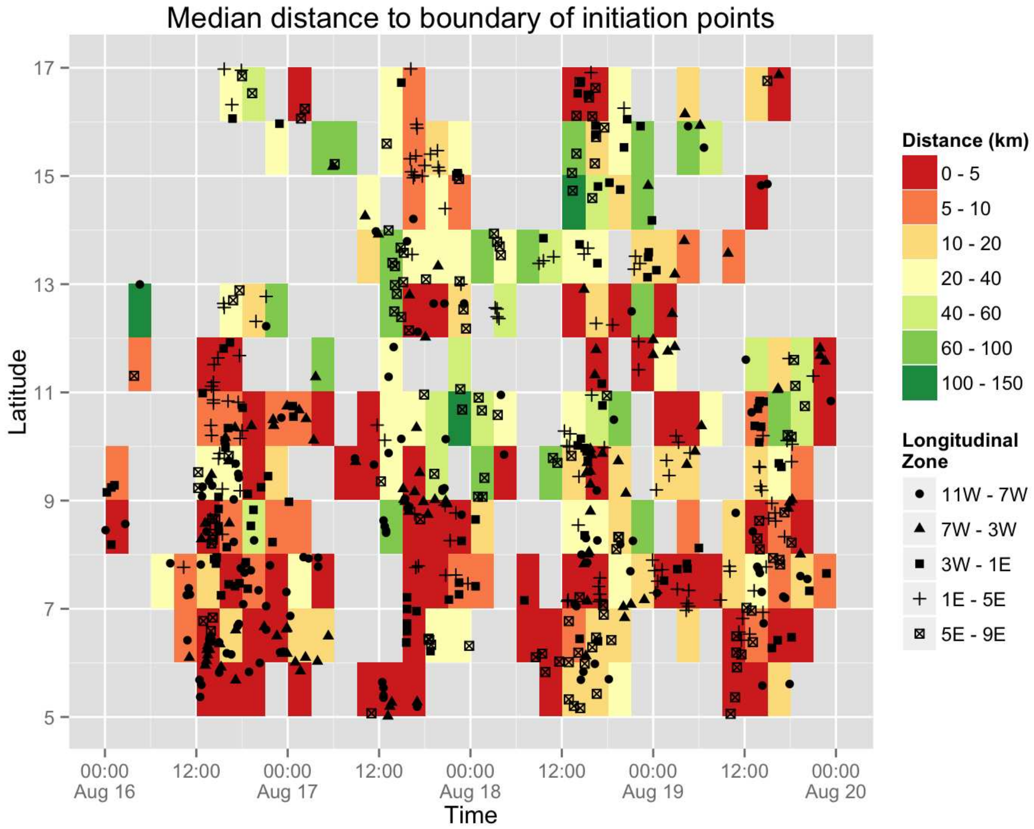

Figure 4 Points of convective initiation (PCI) by time and latitude. Coloured rectangles indicate the median distance in kilometres to a tree-grass boundary for all the PCI that lie within the rectangle, at a temporal resolution of 3 hours (x-axis) and spatial resolution of 1 degree (y-axis). Points are furthermore categorised to show the longitudinal zone in which the point occurs (symbols).

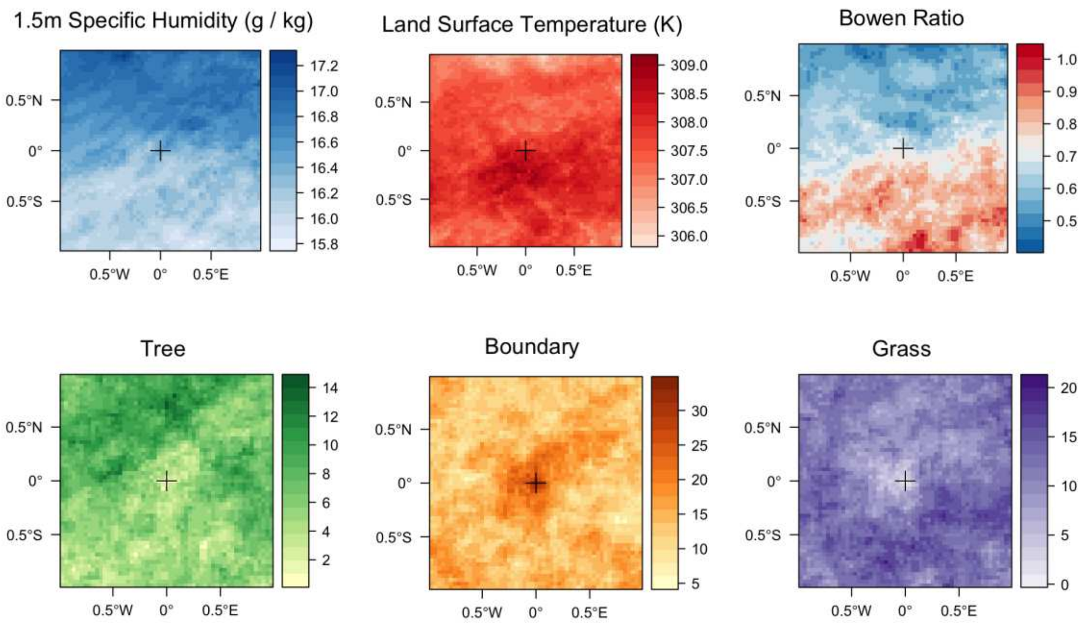

Figure 5 Mean surface conditions (top row) in a 1°x1° box centred on points of convective initiation, rotated to the modal wind direction 90 minutes prior to the initiation of convection. Grid cells north of centre indicate surface conditions upwind, and south of centre indicate conditions downwind. The bottom row shows the total of tree, boundary and grass cover types on the same rotated grids. Results plotted here are for all PCI occurring over boundary in zones 7, 8 and 9 during the afternoon (13:00 to 18:00) period for 4 days of simulation (n=33). Similar plots for other zones are shown in the supplementary material.

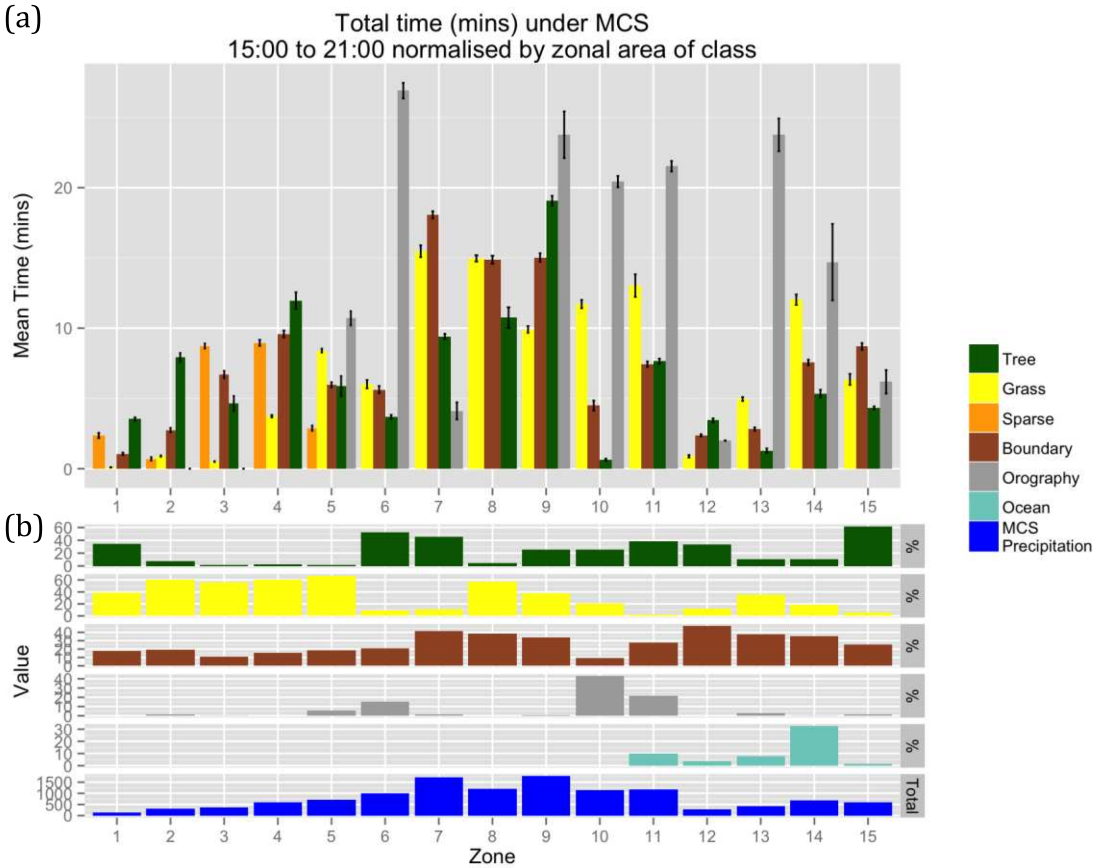

Figure 6 (a) Total time each zonal land cover class is underneath an MCS between 15:00 and 21:00, divided by the zonal area of each land cover class. Error bars indicate the standard error of the mean MCS time. (b) Fractional cover of tree, grass, boundary, orography and ocean grid cells within each zone, and total afternoon MCS precipitation by zone for the full 4 day simulation.

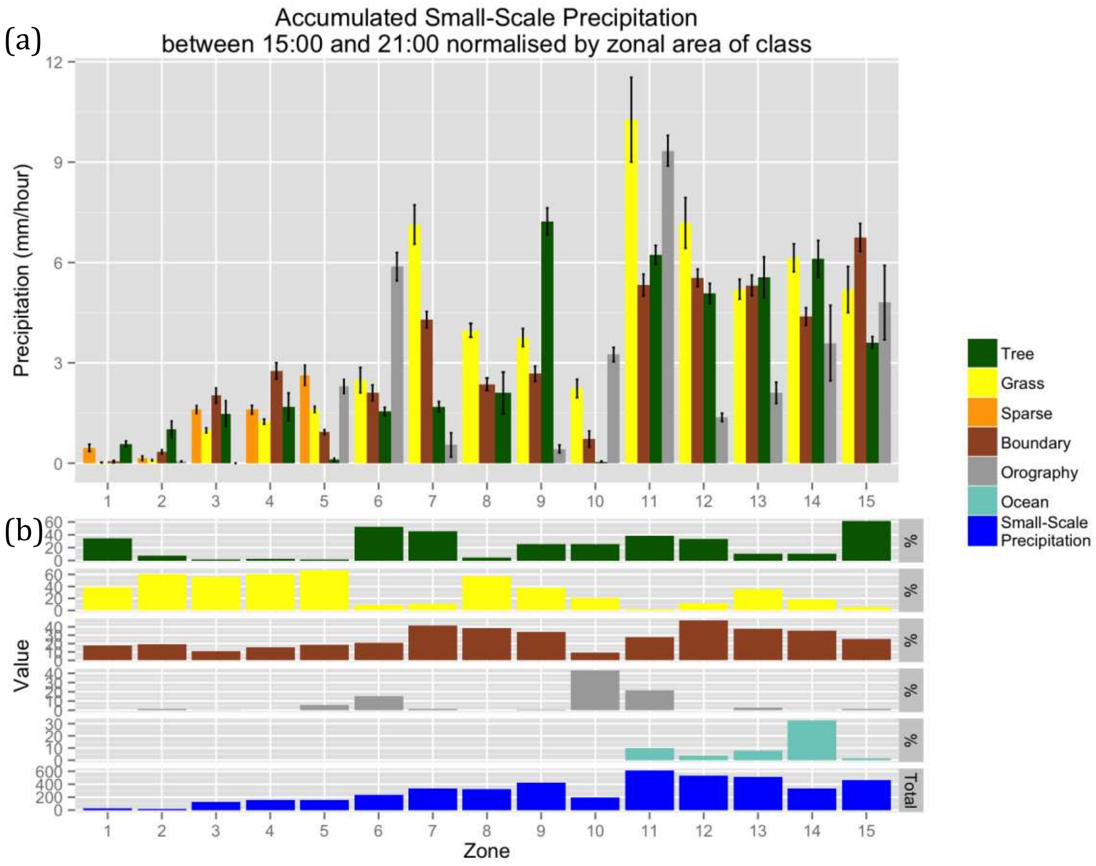

Figure 7 (a) Accumulated small-scale precipitation between 15:00 and 21:00 by zone and land cover class, divided by the total zonal area of that land cover class. Error bars show the standard error of the mean. (b) Fractional cover of tree, grass, boundary, orography and ocean grid cells within each zone, and total afternoon small scale precipitation by zone for the full 4 day simulation.

Supporting Material

Soil moisture

The model used in this study was initialised using the European Centre for Medium-Range Weather Forecasts (ECMWF) soil moisture reanalyses, which we find has a greater frequency of wet soils, and is spatially very smooth compared to modelled soil moisture after several days spinup. As a consequence, in the first few days of this simulation, the soils in the model dry out (by evaporating more moisture to the PBL, and passing moisture to lower soil layers). Previous studies have discarded the first two days of simulation in order to spinup the top layer of soil moisture [*Birch et al.*, 2014]. In this simulation, the change in soil moisture over the spinup period can be seen in figure S1, where the top layer (0-10cm) soil moisture is averaged over a box from 6.5W to 4E and 6N to 22N at hourly model time steps. The shading shows the frequency of grid cells at a given soil moisture at a given time, and contour lines denote the percentile. This shows that there is a higher frequency of grid cells with wet soils (30-40 kg m^{-2}) during the first 2 days of the simulation, and during August 11th the most frequent soil moisture value switches to approximately 10 kg m^{-2}. In the subsequent days, the most frequent soil moisture value gradually reduces further to approximately 5 kg m^{-2} by August 15th, after which it appears to remain stable.

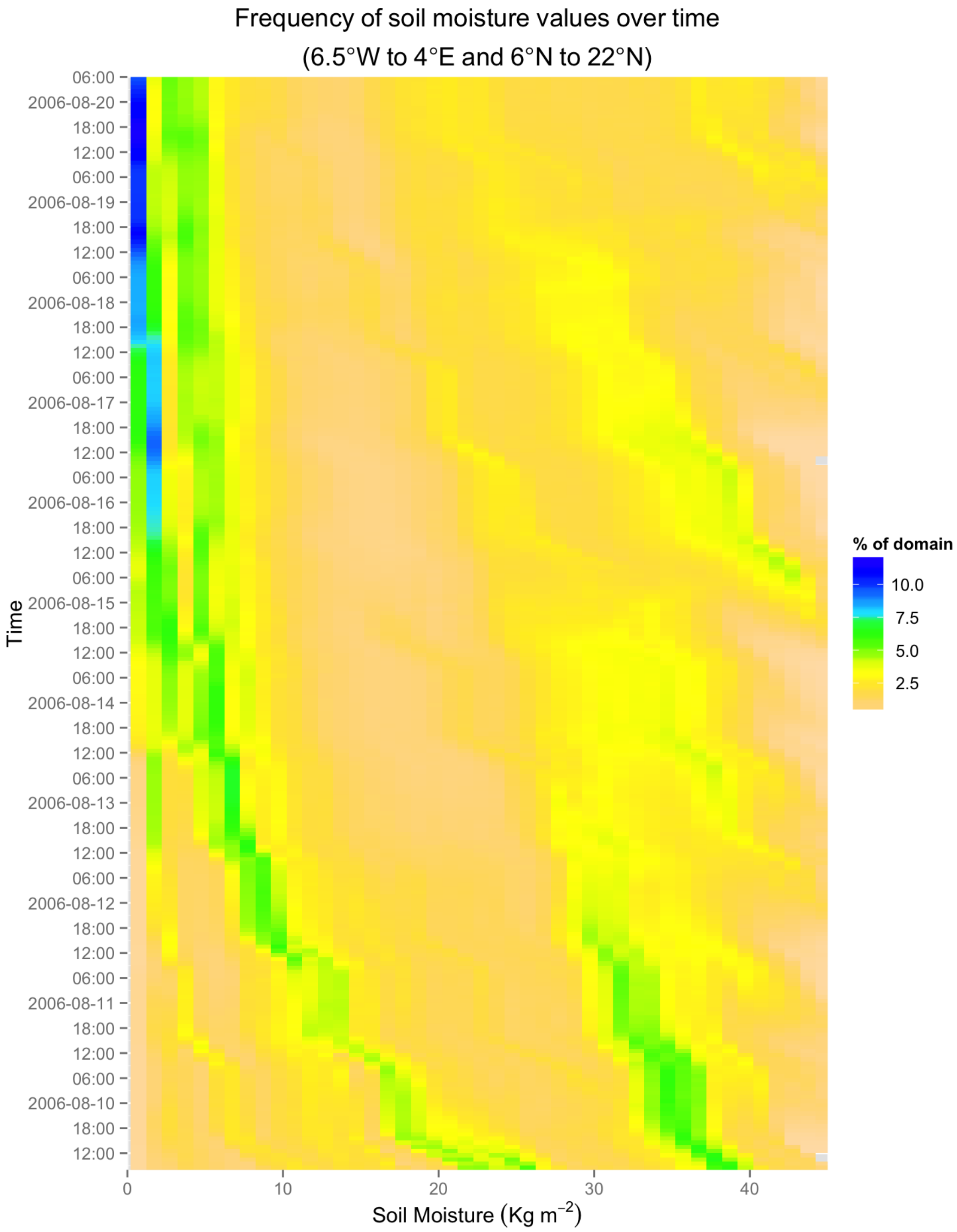

Figure S1 Time varying frequency distribution plot of soil moisture values for the full simulation. Soil moisture values are aggregated over an area which covers the central part of West Africa from the tropical coastal area (Ghana and Cote d'Ivoire) to the arid Sahel (Niger), which lies approximately between 6.5°W to 4°E and 6°N to 22°N. Shading shows the percentage of grid cells in the domain with soil moisture values (binwidth=1Kg m^{-2}) for a given 3 hour period.

Fractional tree cover threshold and surface evapotranspiration

In order to test the most appropriate fractional threshold of tree and shrub cover to use in our classification of 'tree cover', we plotted the mean evapotranspiration for tree fraction bins between 0 and 1, at a frequency of 0.1, for each zone in the study region. Grid cells where precipitation (>1mm/hour) was recorded in the last 24 hours were removed from the analysis in order to remove the influence of wet soils and surface water following rain.

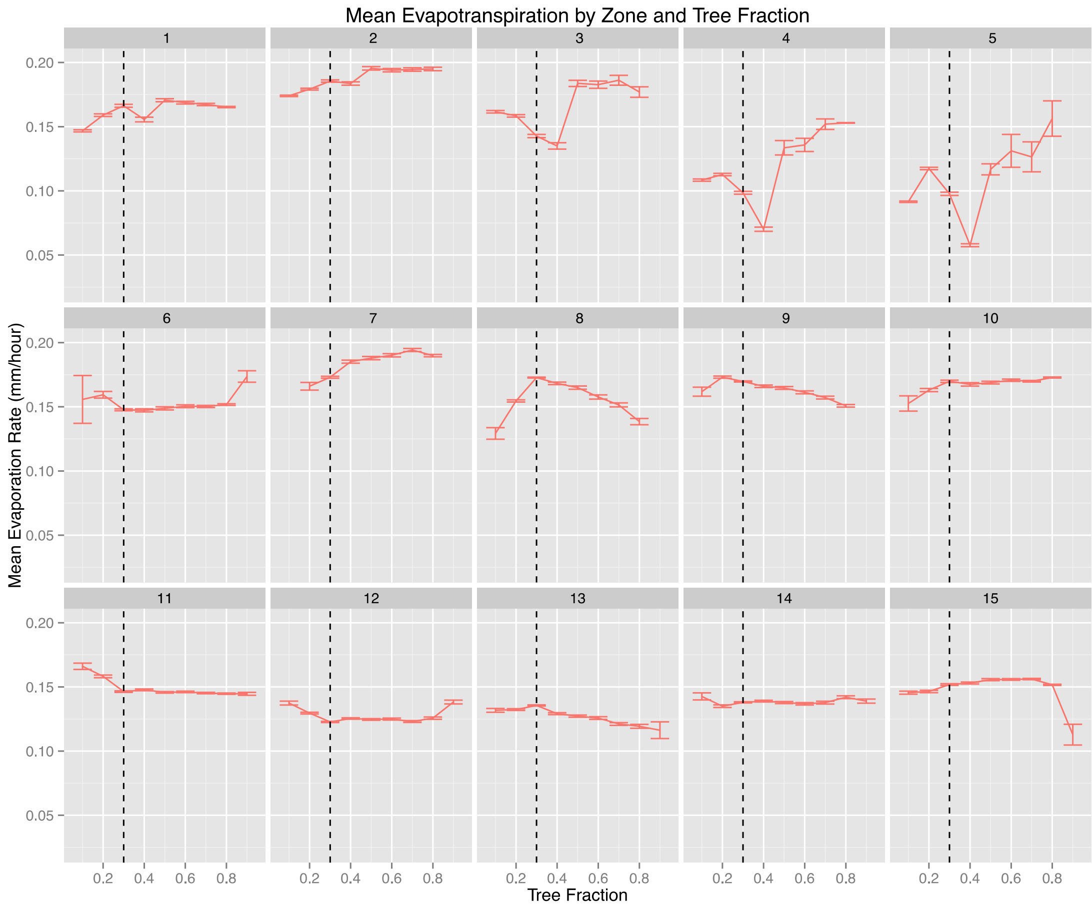

Figure S2 Mean and standard error of total upward surface moisture flux (evapotranspiration) from the land surface, by tree fraction for each zone in the study area, where precipitation did not occur in the previous 24 hours. Vertical dotted lines show the minimum fraction of tree cover permitted in the 'tree cover' class.

Figure S2 shows that, in general, a lower threshold of 0.3 fractional tree cover is appropriate for the definition of a tree class in this study. This provides an important link between the supply of moisture to the atmosphere and the density of tree cover. In the Sahelian part of the study area (zones 1 to 5), evapotranspiration increases with increasing tree fraction. Interestingly, in zones 3, 4 and 5, evapotranspiration is lowest at a tree fraction of 0.4, but increases rapidly for larger tree fractions. Further south, the relationship between tree fraction and evapotranspiration becomes less apparent. In the Sudanian belt (zones 6 to 10), only zones 6, 7 and 10 show a positive relationship between tree fraction and evapotranspiration. In the coastal belt (zones 11 to 15), this relationship is not evident, indicating that there is a ready supply of surface moisture over all cover types.

<u>Surface conditions at 90 minutes prior to initiation of convection</u>

Figure 5 shows the surface conditions rotated to the modal wind direction 90 minutes before the initiation of convection for zones 7, 8 and 9 during the afternoon period. Here, we show similar plots for afternoon (13:00 to 18:00) PCIs over boundary cover in zones 2, 3 and 4 (Figure S3) and zones 12, 13 and 14 (Figure S4). These plots show that the same surface fluxes as found in zones 7, 8, and 9 do not occur near to the coast (zones 12, 13 and 14) and near to the Sahara desert (zones 2, 3 and 4).

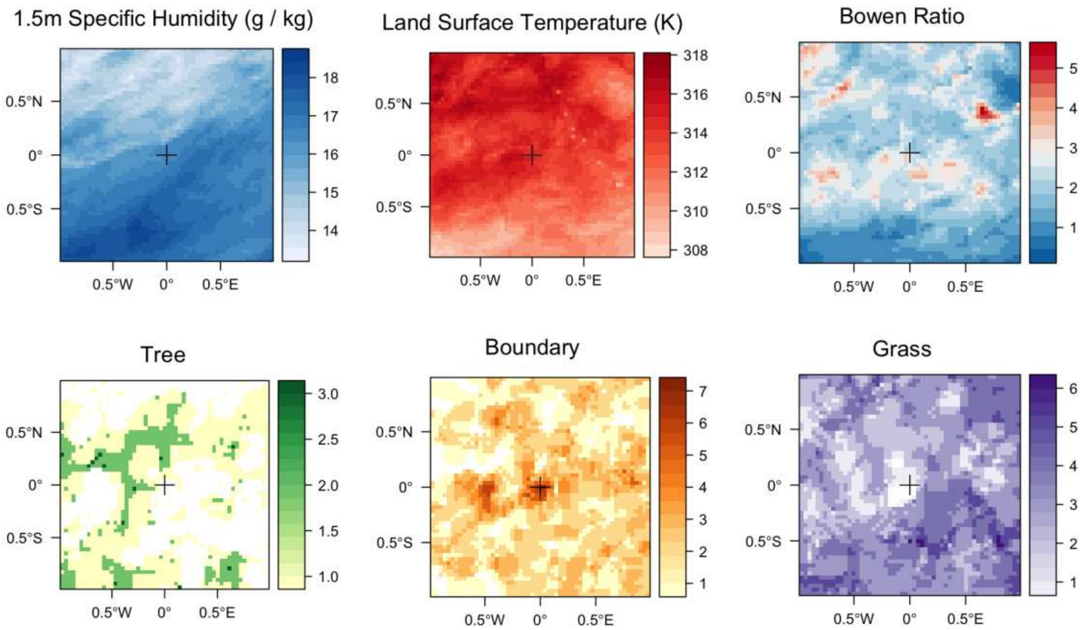

Figure S3 Mean surface conditions (top row) in a 1°x1° box centred on points of convective initiation, rotated to the modal wind direction 90 minutes prior to the initiation of convection. Grid cells north of centre indicate surface conditions upwind, and south of centre indicate conditions downwind. The bottom row shows the total of tree, boundary and grass cover types on the same rotated grids. Results plotted here are for all PCI occurring over boundary in zones 2, 3 and 4 during the afternoon (13:00 to 18:00) period for 4 days of simulation (n=7).

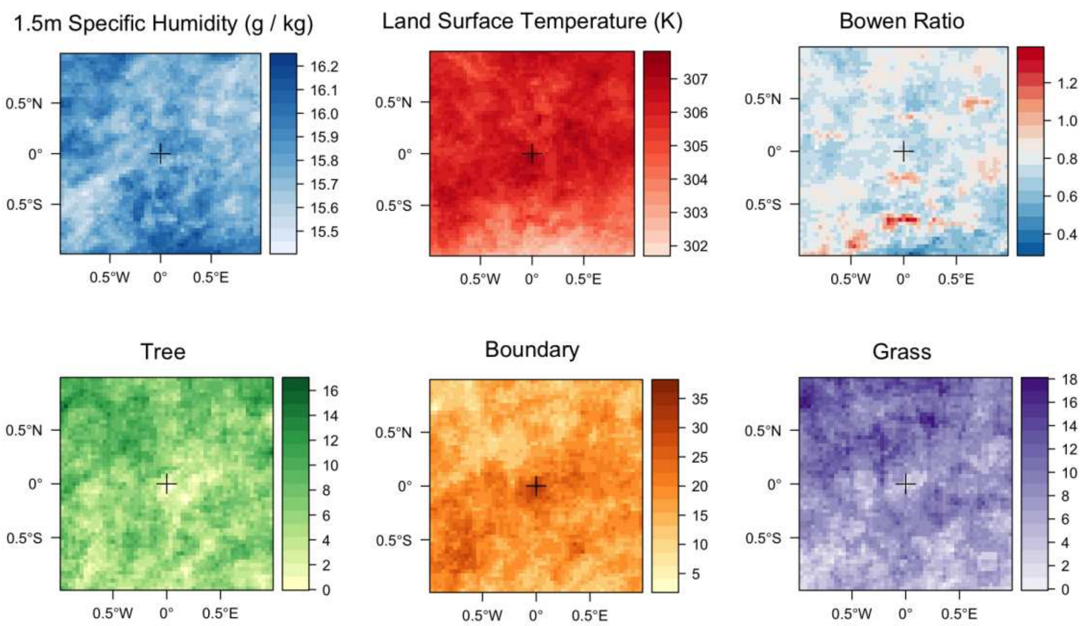

Figure S4 As above, but for zones 12,13 ad 14 (n=36).